Macromolecules

pubs.acs.org/Macromolecules Article

High-Throughput in Situ Characterization of Polymer Crystallization under an Intense Flow, High Pressure, and Cooling Gradient during Injection Molding

Jin Yin,[#] Lu-Feng Deng,[#] Guo-Qi Ma, Feng-Yang Wu, Jia-Zhuang Xu, Xueqin Gao, Fenggang Bian, Jun Lei, Gan-Ji Zhong,* and Zhong-Ming Li*

Cite This: https://doi.org/10.1021/acs.macromol.3c00194 Read Online

ACCESS | Metrics & More | Article Recommendations | Supporting Information

ABSTRACT: Injection molding is a polymer-processing method widely used, which consumes about one-third of global plastics and produces 80% of plastic parts. However, it is still challenging to in situ reveal the structural evolution of polymers during injection molding, which is a long-standing obstacle to understand the relationship of processing−structure−property. This work has first built an in situ investigation system with the aid of a highly brilliant synchrotron X-ray and large experimental space with a length of 30 m, width of 8 m, and height of 6 m, allowing the installation of an industrial-scale injection molding machine. Based on the characterization system, the fast millisecond-resolved structural evolution of general semicrystalline polymers is identified. Various structural types of information including crystallization kinetics, polymorphism, and the growth and orientation of their lamellar crystals under an actual environment of non-isothermal crystallization with a cooling gradient, intense flow, and high pressure during injection molding have been revealed for the first time. The high-throughput feature of the system provides a vital prerequisite for the subsequent establishment of a quantitative database of processing parameter−structure−performance and the precise regulation of polymer aggregation structures, which is valuable for the digitalization and intelligence of the development of the injection molding industry and integration into the Industrial Internet.

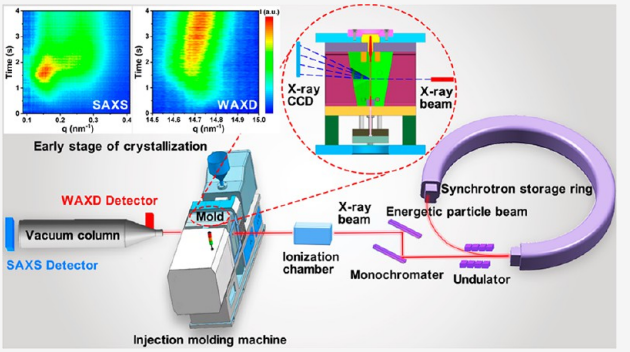

1. INTRODUCTION

Injection molding is one of the most important methods to transform plastic raw materials into products due to the advantages of high automation, a clean environment and high molding efficiency, and the ability to endow products with a complex shape and high dimensional accuracy that are hardly obtained by other polymer processing methods.[1,2] To establish the relationship of "processing parameter−structure−performance", various direct methods are available currently, such as sensors (e.g., thermocouple and pressure sensor) for processing parameter monitoring and standard measurements for the service performance evaluation of injection moldings, respectively. However, in situ or online investigation on the microstructures of injection moldings is still a huge challenge, leading to little understanding in the mechanism of structure formation during injection molding. The difficulty lies in the following: (1) A structural evolution occurs typically within several seconds under a complex thermomechanical environment (typically, a non-isothermal process with a cooling gradient, flow, and pressure field)[3−5] during injection molding where it is highly difficult to catch the kinetics of structural formation by conventional time-resolved characterizations such as in situ Raman (or infrared) spectroscopy,[6] in situ optical microscopy,[7,8] and neutron scattering.[9] (2) The hierarchical nature of polymer structures typically exists.[10−12] The microstructure of an injection article involves the phase morphology (or spherulite for crystalline polymers) ranging from 100 nm to 10 μm, lamellar crystals at a scale of tens of nanometers, and polymorphism crystal structures at a scale of a unit cell with several angstroms, and so on, and the complexity of polymer structures needs a characterization platform for structures. Currently, as a compromised route, an ex situ "black box" mode is used to deduce the structural formation during injection molding, aiming to obtain a semi-quantitative or qualitative empirical processing parameter−structure−property relationship.[13−17] Therefore, a highly time-resolved multiscale characterization technology for injection molding could be promising, which can identify an ultrafast development of a

Received: February 2, 2023
Revised: April 14, 2023

certain microstructure during injection molding and acquire the structural data in a high-throughput manner.

Synchrotron X-ray diffraction (scattering) technology (especially based on the third-generation synchrotron radiation sources) has remarkable characteristics of a high throughput and high penetration (millimeter level of sample thickness) in combination with a state-of-the-art X-ray detector (e.g., cadmium-telluride or silicon detectors), which opens an opportunity for millisecond time-resolved experiments.[18−20] Moreover, various methods including wide-angle X-ray diffraction (WAXD), small-angle X-ray scattering (SAXS), and ultrasmall-angle X-ray scattering (USAXS) cover a wide scale of hierarchical structures of polymers. For instance, in situ two-dimensional WAXD/SAXS (2D-WAXD/SAXS) can be implemented to obtain multiscale information of crystalline structures simultaneously, including the crystal size and d spacing at an angstrom scale, long period of lamellae at a nanometer scale, polymorphism, and orientation of multiscale structures. Therefore, the synchrotron X-ray scattering technology is capable of polymer structural characterization and could become an ideal tool for obtaining polymer structural information during injection molding in a high-throughput way.

Synchrotron X-ray in situ characterization in conjunction with a bench-scale instrument such as a rotational rheometer,[21] small extruder,[22] and micro-injection molding machine[4,5,23] has been used to study the structural formation processes of polymers under a thermomechanical environment. However, in situ experiments of industrial-scale injection molding have not yet been reported, and direct guidance for injection molding of certain polymers is lacking. To combine the synchrotron X-ray in situ characterization with injection molding installation-covering processing parameters in industry is still challenging. The space limitation for industrial equipment installation in beamline, the mold design for in situ characterization, and the alignment of X-ray beams are also technical issues to be solved first.

The current work attempts to realize in situ characterization for industrial-scale injection molding based on synchrotron X-ray diffraction and scattering with a millisecond time resolution. Furthermore, by using the system, the crystallization kinetics, polymorphism formation, and folded-chain lamellar crystals of the semicrystalline polymer during the injection molding are investigated. Finally, the system is tested to determine processing windows of injection molding for a specific polymer in a high-throughput manner. Moreover, the development of this in situ investigation system is undoubtedly conducive to the establishment of a "processing parameter−structure−performance" database with high efficiency, which is highly expected to provide direct guidance on the optimization of injection moldings' performance in industry.

Meanwhile, in the context of Industry 4.0 and the Industrial Internet, injection molding has been developed toward digitalization and intellectualization, that is, so-called intelligent injection molding.[24,25] A database of "material composition−processing parameter−structure−performance"[26,27] can be established by further utilization of the in situ characterization system set up in this work, and the relationship of the processing−microstructure−performance can be quantified by advanced big data analysis methods.[27−31] Future work and outcomes based on this system could provide a desirable way to realize intelligent injection molding for autonomously seeking optimum parameters of material formulation and processing for the required service performance.

2. EXPERIMENTAL SECTION

2.1. Materials. The materials used in this study include two kinds of high-density polyethylene (HDPE), namely, HDPE-1 (China Petroleum & Chemical Corporation) and HDPE-2 (Saudi Basic Industries Corporation), and two kinds of isotactic polypropylene (iPP), namely, iPP-1 (Shanghai SECCO Petrochemical Co., Ltd.) and iPP-2 (ExxonMobil Corporation). The basic information of the four polymer materials is listed in Table 1, including the trademark, polymer density (ρ), and melt flow index (MFI). In addition, iPP-1/β, namely, a mixture of iPP-1 and a β nucleating agent (β-NA, branded TMB-5, an arylamide derivative provided by Shanxi Provincial Institute of Chemical Industry, China with a mass fraction of 0.2 wt %), was also used.

Table 1. Basic Information of Four Raw Polymers

	trade mark	ρ (g/cm^3)	MFI (g/10 min)
HDPE-1	5000S	0.954	0.82 (190 °C, 2.16 kg)
HDPE-2	CC3054	0.954	30.0 (190 °C, 2.16 kg)
iPP-1	S1003	0.900	3.0 (230 °C, 2.16 kg)
iPP-2	3155E3	0.900	36.0 (230 °C, 2.16 kg)

2.2. Sample Preparation. The iPP-1 containing 0.2 wt % β-NA (iPP-1/β) was prepared by melt blending of TMB-5 and iPP-1 using a twin-screw extruder. The screw speed was 87.5 rpm, and the temperatures from the hopper to the die were set at 150, 160, 170, 175, 175, 180, 180, and 180 °C, respectively.

The injection molding parameters were set as follows: for HDPE, the temperatures from the barrel to the nozzle were set at 135, 175, 180, and 170 °C in turn; for iPP and iPP-1/β, the temperatures were set at 185, 200, 200, and 190 °C. In order to explore the effect of the processing temperature on the crystallization behavior of the iPP-1/β sample, we set three processing temperatures, that is, 200, 215, and 230 °C. Additionally, the injection rates were set at 25, 50, 100, and 200 mm/s; packing pressures were set at 25, 50, 100, and 200 MPa; packing and cooling times were 2 and 10 s, respectively.

2.3. In Situ X-ray Characterization of Crystallization during Injection Molding. The in situ SAXS/WAXD characterization platform for injection molding was built on the beamline BL10U1 of the Shanghai Synchrotron Radiation Facility (SSRF, Shanghai, China). The beam size was 379 μm (horizontal direction) × 341 μm (vertical direction). The wavelength of the X-ray source (λ) was 0.1240 nm. The 2D-SAXS and WAXD images were collected by a detector of PILATUS3 2M with a pixel array of 1475 × 1679 pixels and a detector of PILATUS3 900K with a pixel array of 981 × 1043 pixels, respectively. Both detectors have a pixel size of 172 × 172 μm^2 with a sensor thickness of 450 μm. As for the SAXS/WAXD characterization of HDPE, the distances from the sample to the detectors were 5454.6 and 785 mm, respectively. For the SAXS and WAXD measurements of the iPP and iPP-1/β mixture, the distances were 5454.6 and 838.2 mm, respectively. The X-ray exposure time of synchrotron radiation was 0.025 s.

The SAXS and WAXD data were calibrated with a bull collagen fiber and HDPE standard, respectively. The one-dimensional (1D) SAXS/WAXD intensity profiles were obtained from circular integration of the 2D-SAXS/WAXD patterns after subtracting the air background. The contour maps were drawn with the intensity, q (the module of the scattering vector), and time data of the obtained 1D-SAXS/WAXD curves. The intensity versus time curves were drawn by extracting the intensity corresponding to the q value of the polymer crystal planes. The contour maps of the crystallization time were plotted by counting the time when the intensity of polymer crystal planes increases until equilibrium in different processing conditions.

https://doi.org/10.1021/acs.macromol.3c00194
Macromolecules XXXX, XXX, XXX−XXX

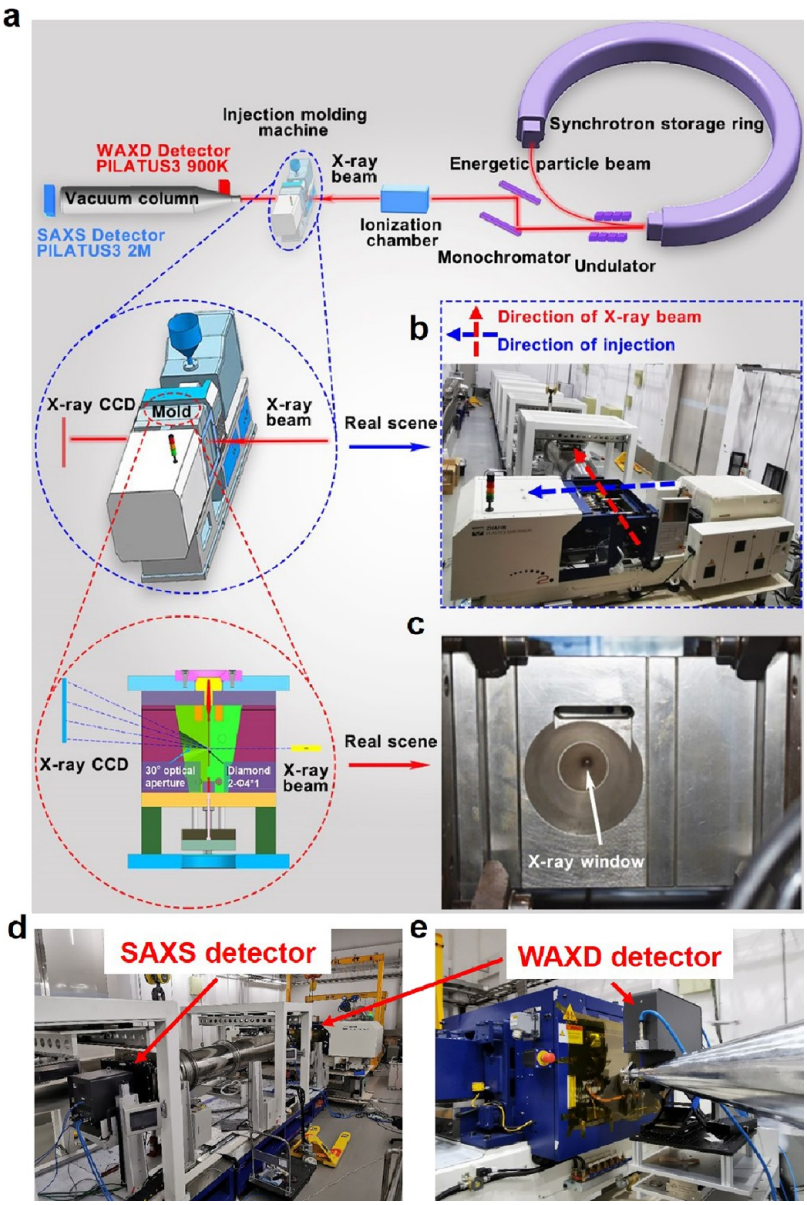

Figure 1. In situ characterization system for injection molding. (a) Schematic diagram of the in situ characterization system for injection molding. (b) Showing a real scene. The blue dashed arrow represents the direction of injection, and the red dashed arrow represents the direction of the X-ray beam. (c) Picture of the mold. (d, e) Site photographs of the apparatus. (d) Showing the detector for SAXS. (e) Showing the detector for WAXD.

More details about the simulation analysis of the injection molding process and the processing methods of other data are provided in the Supporting Information.

3. RESULTS AND DISCUSSION

3.1. High-Throughput Characterization Platform for Injection Molding. In order to realize the in situ investigation of injection molding, injection molding equipment combined with highly time-resolved detectors is required to reveal the extremely fast process. Previously, in situ investigation systems of injection molding using an optical device and ultrasonic technique are reported. For instance, near-infrared spectroscopy (NIR) is utilized to monitor injection molding with the aid of two optical fiber probes attached to the injection molding machine.[6] The optical device is inserted in the injection mold cavity to monitor the non-isothermal crystallization of polypropylene by detecting the change of transparency properties that resulted from crystallization during injection molding,[7] and an ultrasonic technique is also used to monitor the injection molding by measuring the velocity and attenuation of the ultrasound in the polymer.[32] Compared to NIR and ultrasound technologies, X-ray scattering can reveal the polymeric structure (especially the crystalline structure) in detail. Pioneer works realize the combination of micro-injection equipment with synchrotron SAXS[4,5] and laboratory-scale injection molding machines with synchrotron WAXD.[23] These injection molding machines with small sizes utilize an injection plunger, which is not widely used in industry due to the limited ability for mixing and plasticization of raw materials. In order to achieve the in situ multiscale investigation of injection molding with the processing parameters fully used in industry, in this work, a reciprocating screw injection molding machine is set up with a maximum injection pressure of 280 MPa, a maximum injection

https://doi.org/10.1021/acs.macromol.3c00194
Macromolecules XXXX, XXX, XXX−XXX

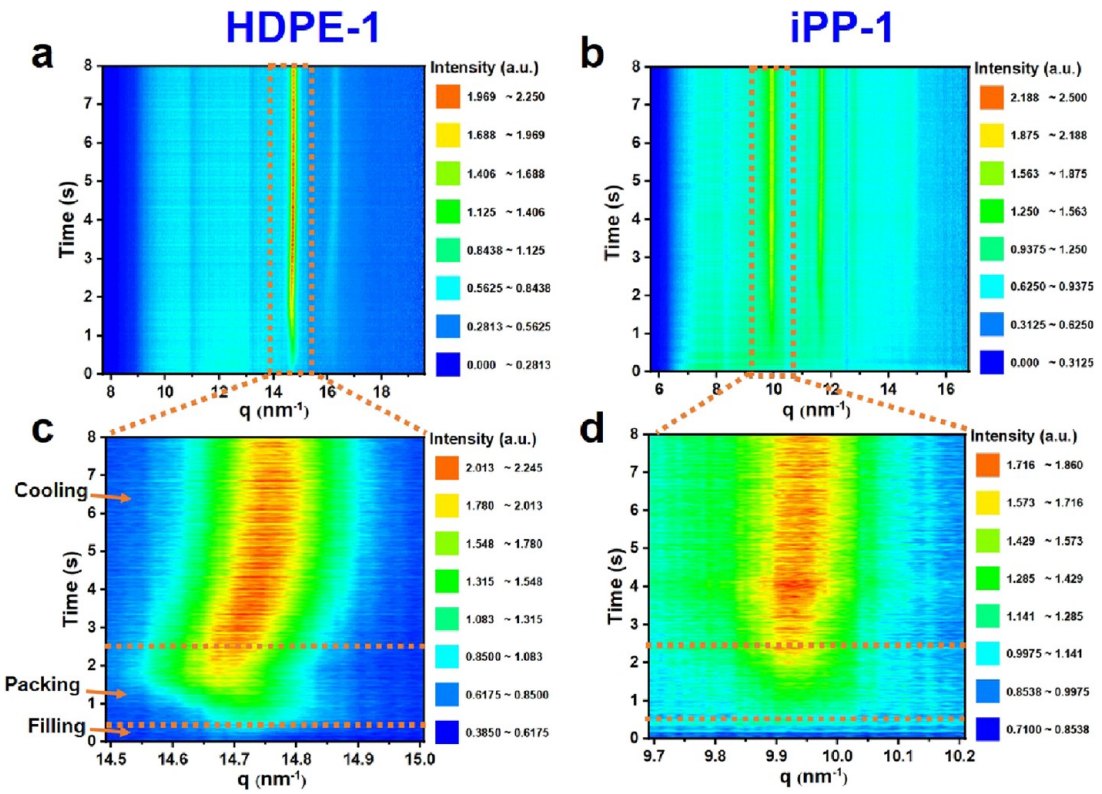

Figure 2. In situ WAXD showing the crystallization kinetics of various polymers in cavity during injection molding. (a) HDPE-1. (b) iPP-1. (c, d) Local enlargements of a and b, respectively (injection rate: 100 mm/s; packing pressure: 200 MPa).

molding rate of 350 mm/s, and a maximum mold temperature of 180 °C as well as a shear rate with an order of magnitude of 10^4 s^{-1} (Figure 1b). The variables of processing parameters basically cover the current industrial level of injection molding. Additionally, the design of the injection mold is vital for the in situ characterization system for injection molding, that is, a tapering hole with a 30° opening angle is designed to avoid interferences with the scattered X-ray and diamond windows are used to seal the high-pressure polymer melt (Figure 1c). The injection molding equipment is installed in the industrial experiment station of SSRF, which has high-throughput characterization capability with an electron beam energy of 3.5 GeV, high X-ray photon flux (>10^{13} phs/s), ultrasmall spatial resolution (less than 50 μm), and wide scale measurement ranging from 0.1 nm to 1 μm, which is capable of identifying hierarchically crystalline structures of semicrystalline polymers at a scale of a unit cell with several angstroms, lamellar crystals at tens of nanometer scale, and so on. Moreover, a large experimental space with a length of 30 m, width of 8 m, and height of 6 m is available, ideally meeting the space requirement for the combination of a synchrotron radiation X-ray diffraction (scattering) facility and industrial-scale injection molding machine. Two detectors are installed to simultaneously acquire SAXS and WAXD signals of polymer crystals (Figure 1d,e), operating at frame rates of up to 500 Hz with a single photon counting module and count rates of up to 10^7 phs/s/pixel. Meanwhile, to conduct the alignment of the X-ray characterization system and injection molding system, a precise positioning stage is also designed to load the injection molding machine with a weight of ∼3.5 tons and to realize the micrometer-level motion so that the X-ray can pass accurately through the two diamond windows in the mold (Figure 1a). With a combination of aforementioned considerations, we have built the high-throughput in situ characterization platform for capturing the extremely fast process of microstructure formation during injection molding. The crystallization kinetics, polymorphism evolution, and growth and orientation of folded-chain lamellar crystals of semicrystalline polymers are shown as follows. General-purpose polymers are used in this work due to their huge consumption in injection molding industry, including two kinds of HDPE (denoted as HDPE-1 and HDPE-2), two kinds of iPP (denoted as iPP-1 and iPP-2), and the mixture of iPP-1 and β-NA (named iPP-1/β).

3.2. Polymer Crystallization Kinetics during Injection Molding. Crystallization kinetics reveals the nucleation and crystal growth of semicrystalline polymers,[33,34] which can obtain important parameters such as the induction time of nucleation, overall crystallization rate (G), and growth dimensionality of the crystals in order to understand crystallization in details. The current study on polymer crystallization kinetics has mainly involved individual or two parameters of external fields including the temperature,[34−36] pressure,[37] and shear rate,[38,39] which is not fully consistent with the complex thermomechanical fields during injection molding. The complex thermomechanical field of fast cooling rates, high pressures, and strong flows during injection molding makes it extremely difficult to identify the crystallization behavior of polymers in detail.[2] Herein, we select the representative commodity polymers of HDPE-1 and iPP-1 to investigate the crystallization kinetics during injection molding by the in situ characterization system.

Figure 2a,b and Movies S1 and S2 demonstrate that the rapid crystallization processes of HDPE-1 and iPP-1 during injection molding are successfully monitored, respectively. The

https://doi.org/10.1021/acs.macromol.3c00194
Macromolecules XXXX, XXX, XXX−XXX

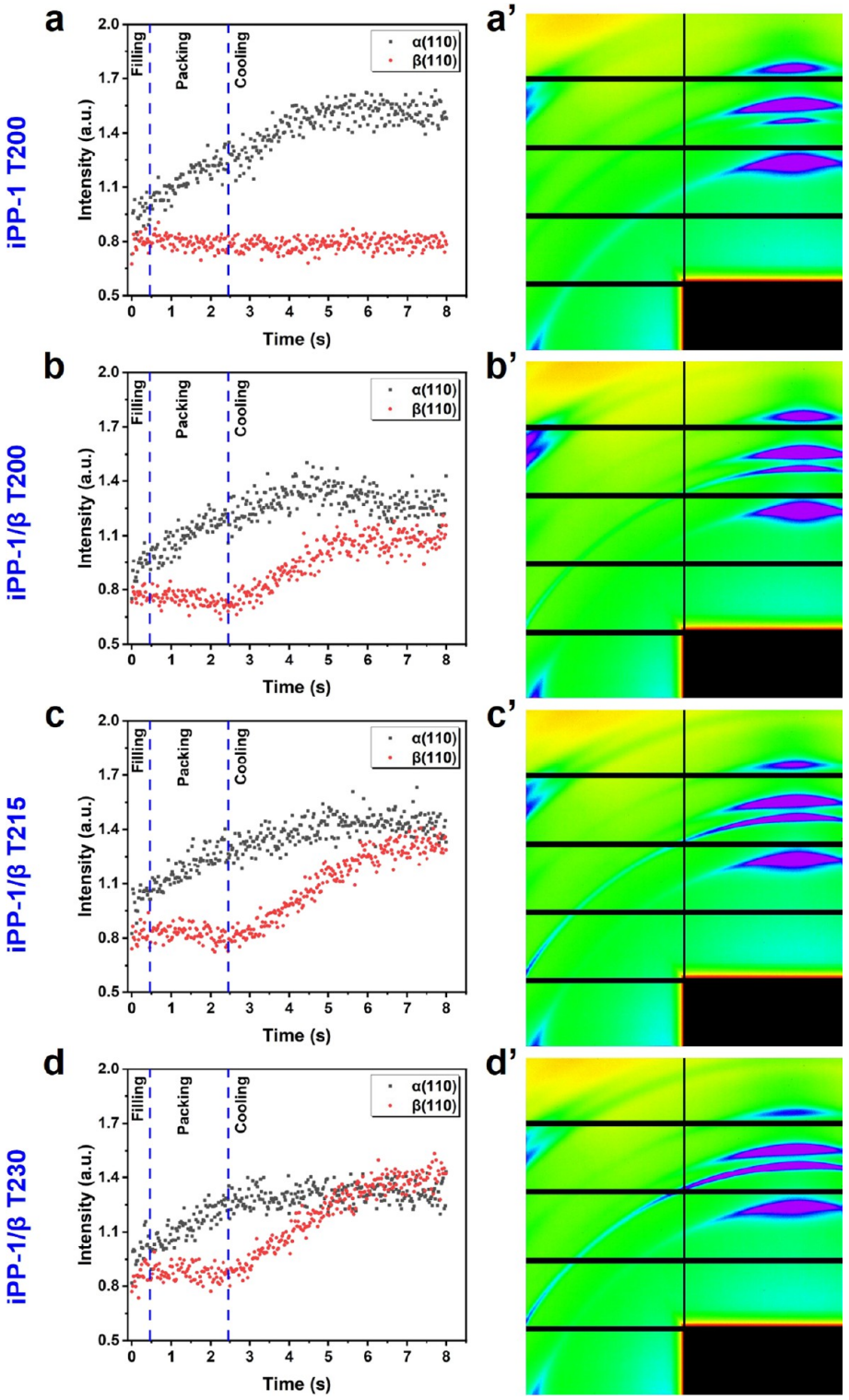

Figure 3. Competitive growth of α and β crystals of iPP-1 and iPP-1/β during injection molding at different melt-processing temperatures (T). (a) iPP-1 at 200 °C. (b) iPP-1/β at 200 °C. (c) iPP-1/β at 215 °C. (d) iPP-1/β at 230 °C. (a′−d′) Final 2D-WAXD patterns of a−d, respectively (X-ray exposure time of 1 s, injection rate: 100 mm/s, and packing pressure: 100 MPa).

diffraction intensities of the orthorhombic phase (110) plane for HDPE-1 and the diffraction intensities of the α (110) plane for iPP-1 are selected to describe the characteristics of their crystallization kinetics due to its high intensity. As highly crystalline polymers (e.g., polyethylene and polypropylene), it is found that crystallization starts as soon as the samples are injected into the cavity of the injection mold, and the crystallization induction period is quite short (<0.5 s), and the whole crystallization is completed within 4 s. The in situ characterization system can directly identify the crystallization rate of HDPE-1 and iPP-1 crystals (Figure S2). Surprisingly, the (110) planes of both HDPE-1 and iPP-1 have two growth processes. For HDPE-1, the G of the first process within 1 s is 0.719 s^{-1}, while the second process at 1−4 s is a relatively

https://doi.org/10.1021/acs.macromol.3c00194
Macromolecules XXXX, XXX, XXX−XXX

lower G of 0.306 s^{-1}. For iPP-1, the G of the first process is 0.772 s^{-1} within 0.5 s, while the G of the second process at 0.5−4 s presents a lower G of 0.146 s^{-1}. Figure S1 reveals the complex external fields existing during injection molding based on finite element simulation. One can see that, during the filling stage, only the skin layer (region of approximately a thickness of 100 μm) with a temperature less than the melting point could have an appropriately thermal environment for crystallization, and the intensive shear flow (above 10^4 s^{-1}) exists within 0.3 s and its maximum is located in the middle layer (region of an approximate thickness of 150 μm). Meanwhile, a high pressure between 100 and 175 MPa is imposed on the melt during crystallization, indicating that the initial crystallization during injection molding occurs under a combined field of an intense shear rate and high pressure. At the packing stage, the high packing pressure (maximum to 175 MPa) increases the nucleation barrier,[40] which slows down the crystallization rate and subsequent growth of polymer crystals. In the cooling stage, the temperature of different layers of HDPE-1 or iPP-1 successively decreases to ca. 25 °C, which should stop the crystallization. With the aid of simulation results, we believe that the first process has a higher crystallization rate for the (110) planes of HDPE-1 and iPP-1 due to the intensive shear and, subsequently, the second process presents a lower crystallization rate because of the inhibitive effect of the high pressure on crystallization and relaxation of a shear-induced orientation. In comparison, HDPE-1 and iPP-1 have similar crystallization rates at the first process, while the slower crystallization rate for iPP-1 at the second process originates from the presence of methyl groups in the main chain, and the formation of a helical conformer as a precursor of crystallization needs more time for regular arrangement of the crystallizable segments.[34]

Intriguingly, the lattice spacing of the α (110) plane of HDPE-1 and iPP-1 varies during injection molding (Figure 2c,d). Specifically, the lattice spacing between the planes (d_{hkl}) is determined using the Bragg equation: $d_{hkl} = \lambda/2 \sin\theta = 2\pi/q$ (λ is the wavelength, θ is half of the diffraction angle, and q is the scattering vector).[41] It is obviously observed that the three stages for the variation of the lattice spacing exist during HDPE-1 injection molding. At the filling stage, it decreases from 0.4280 nm at q = 14.6803 nm^{-1} to 0.4266 nm at q = 14.7285 nm^{-1}. Subsequently, it distinctly increases to 0.4286 nm at q = 14.6598 nm^{-1} during the packing stage, and then, it reduces again to 0.4254 nm at q = 14.7701 nm^{-1} with the proceeding of the cooling stage (Figure S3a−c). In contrast, at the packing stage, the lattice spacing of iPP-1 barely changes and subsequently reduces slightly from 0.6327 nm at q = 9.9307 nm^{-1} to 0.6315 nm at q = 9.9496 nm^{-1} (Figure S3d−f) with the increase of the cooling time. When the hot melt of HDPE-1 is injected into mold, the lattice spacing tends to reduce because of flow-induced crystallization of HDPE-1 and subsequent compact stacking of oriented chain segments; in addition, the material shrinkage due to the cooling process also leads to the decline of the lattice spacing. Unexpectedly, the lattice spacing increases within the packing stage, ranging from 0.5 to 2 s, revealing a specific formation of the hexagonal phase of polyethylene at the packing stage with the aid of high pressure and high temperature, which consists of the parallel stacking of the conformationally disordered molecular chains with a large lattice spacing.[42−44] Differently, the lattice spacing of the α crystal of iPP-1, which has only one monoclinic phase with alternating molecular chains of left- and right-handed helical conformations, is found to monotonously decrease due to material shrinkage during the cooling process of injection molding.

3.3. Polymorphism Evolution of the Semicrystalline Polymer during Injection Molding. The polymorphism formation of semicrystalline polymers under a complex thermomechanical environment during injection molding is investigated by the in situ characterization system of injection molding. iPP exhibits a typical polymorphism including α, β, and γ forms, which is selected in this work. Among them, the β crystal growth of iPP is strongly relative to the shear flow,[45,46] crystallization temperature,[47] and nucleation agents.[48] Moreover, β-NA is used to induce a high content of the β crystal in industry, which is beneficial to ameliorate the toughness of iPP products (including impact strength and elongation at break).[49−52] However, it is still unclear how the coupling effect of the complex thermomechanical field and heterogeneous nucleating agent affect the formation of β crystals in injection molding. The two-stage growths of iPP-1 with β-NA (iPP-1/β) during injection molding are found for the first time by the in situ characterization system (Figure 3b−d and Movie S3), one occurs in the filling stage and another in the cooling stage of injection molding. For the first stage, iPP-1 and iPP-1/β have a similar growth tendency (Figure 3a), it is suggested that the first-stage growth of β crystals is mainly related to the thermomechanical environment during injection molding rather than β-NA. We consider that the formation of β crystals at the first stage is attributed to the shear effect at the filling stage of injection molding, that is, the shear-induced formation of α row nuclei and then β crystals epitaxially grow on the formed α row nuclei.[39,45,53] During the cooling stage, one can see a more obvious growth stage of β crystals for iPP-1/β, which is prominently induced by the β-NA as compared to iPP-1. We calculate the relative contents of the β crystal (K_β) after deconvoluting the diffraction peaks in the 1D-WAXD profiles. The addition of β-NA facilitates the increase of the K_β of iPP-1 from 3.74 to 18.72% after the second growth stage (Figure S4a). In addition, the comparison of iPP-1 and iPP-1/β at 200 °C shows that the addition of β-NA decreases the (110) plane crystallization rate of the α crystal from 0.113 to 0.091 s^{-1} (Figure S4b), which indicates that the addition of β-NA would restrain the growth of the α crystal. This is consistent with the findings of previous studies in that β-NA provides a mass of β nucleating sites for the growth of β crystals, which greatly suppresses the growth space of α crystals and limits the growth of α crystals.[54−56]

It is reported that the solubility of β-NA in iPP melt enhances at a high temperature of thermal treatment, which improves the nucleation efficiency and enhances the content of the β crystal.[57−59] At the same time, a higher temperature is also conducive to the self-assembly of β-NA dissolved in iPP melt during cooling, forming a fibrous crystal structure with a high aspect ratio, thereby inducing more β crystals to epitaxially grow on their surfaces.[60] For the case of injection molding, the in situ characterization system verifies that the growth of β crystals in iPP-1/β is significantly affected by the melt temperature (Figure 3), which is consistent with the previous understanding. When the melt temperature increases from 200 to 230 °C, the saturated diffraction intensity of β crystals gradually increases compared to that of α crystals (Figure 3a−d). In 2D-WAXD patterns of final parts (Figure 3a′−d′), the remarkable enhancement in the intensity of the β crystals' diffraction arc also verifies the synergistic effect of β-

https://doi.org/10.1021/acs.macromol.3c00194
Macromolecules XXXX, XXX, XXX−XXX

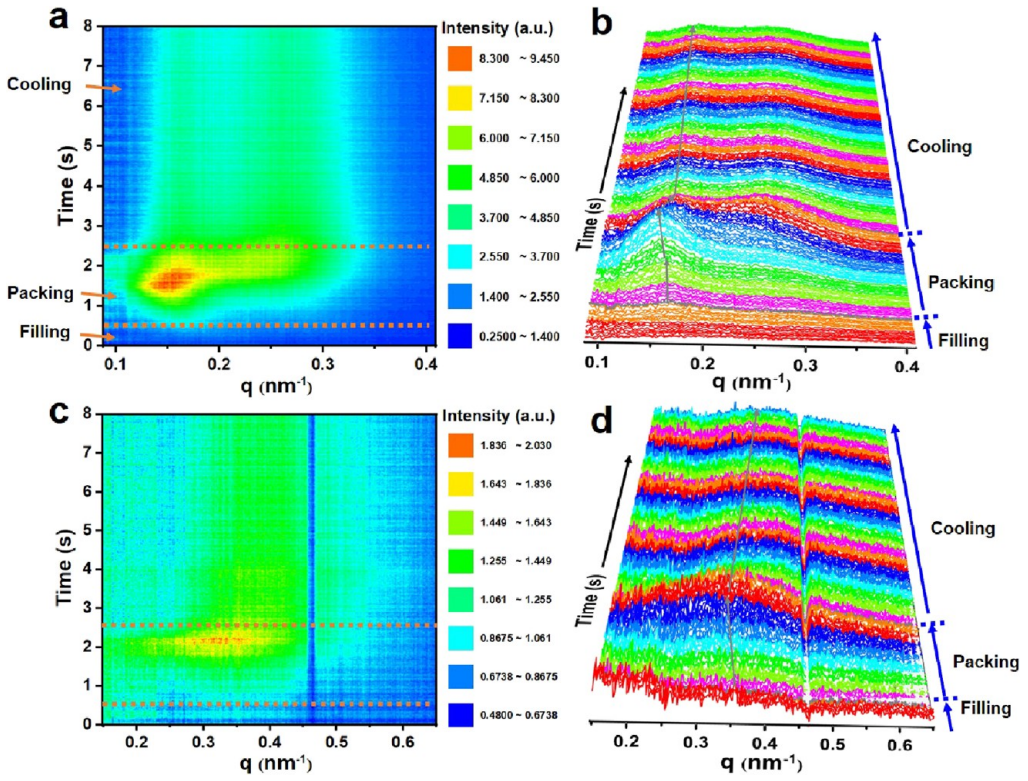

Figure 4. Growth of lamellar crystals during injection molding revealed by in situ SAXS characterization. (a) HDPE-1 and (c) iPP-1. 1D-SAXS curves of (b) HDPE-1 and (d) iPP-1 (Injection rate: 100 mm/s; packing pressure: 200 MPa).

NA and melt temperature to produce a higher content of oriented β crystals. Specifically, there is a significant increase in β crystal content from 18.72% for the case of 200 °C to 25.04% for 215 °C and finally to 31.07% for 230 °C (Figure S4a). Meanwhile, the (110) plane crystallization rates of β crystals at 200, 215, and 230 °C are 0.121, 0.142, and 0.152 s^{-1}, respectively (Figure S4b), indicating that the increase of the melt temperature effectively promotes the growth of the β crystal.

Another novel phenomenon is that the packing pressure has a significant influence on the growth of β crystals (Figure S5), the growth of β crystals induced by β-NA seems to start after the ceasing of packing, and the saturated content of β crystals decreases with the elevation of packing pressure. The K_β is 28.35% at 25 MPa of the packing pressure, which is significantly higher than 18.72% at 100 MPa and 10.79% at 200 MPa (Figure S5d). We suggest that the nucleation barrier of β-iPP is higher than that of α-iPP under high pressures, which will facilitate the preferential growth of α crystals. Moreover, the maximum growth rate of the α crystal is found to increase with increasing the pressure, leading to detrimental conditions for β crystal growth.[61] After the release of the packing pressure, the heterogeneous nucleation of β-NA provides abundant nucleation sites for the nucleation of β crystals, and a large number of β crystals could be quickly obtained.[40] According to this observation, it shows that the lower the packing pressure of injection molding, the more favorable the formation of β crystal, which should be valuable information to guide the injection molding processing of the toughened iPP system by β crystals.

3.4. Growth and Orientation of Lamellar Crystals during Injection Molding. The growth process of folded-chain lamellar crystals for HDPE-1 and iPP-1 is also monitored by the in situ characterization system of injection molding (Figure 4a,c and Movies S4 and S5), respectively. In situ investigation on the growth of HDPE-1 lamellar crystals (Figure 4a) clearly reveals that two types of lamellar crystals with different thicknesses form under the complex thermo-mechanical fields during injection molding, whereas only one type of iPP-1 lamellar crystal is identified, which is also visualized by the 2D-SAXS patterns and the corresponding 1D-SAXS curves of HDPE-1 and iPP-1, respectively (Figure S6a–d). To further verify the existence of the two types of HDPE-1 lamellar crystals and one type of the iPP-1 lamellar crystal, differential scanning calorimetry (DSC) measurements of injection molded HDPE-1 and iPP-1 are carried out (Figure S7a,b). The DSC curves show that the raw material of HDPE-1 has one melting peak of ~130 °C, while the injection molded sample has a shoulder at a higher temperature (around 140 °C) except for the main melting peak around 130 °C, confirming two types of lamellar crystals for HDPE-1 induced by the complex thermomechanical field during injection molding. For HDPE-1, the long period (d_{ac}) and thickness (d_c) of the thick lamellae are 43.8 and 34.2 nm ($d_{ac}-d_a$), whereas the d_{ac} and d_c of the thin lamellae are 23.6 and 14.0 nm, respectively (Figure S6e). We believe that the thick lamellae are related to the kebab structure induced by the shish structure resulting from the strong shear flow-induced crystallization at the early stage further promoted by high pressure,[62,63] and subsequently, the thin one occurs corresponding to lamellae epitaxially growing on the shish-kebab structure. Moreover, iPP-1 has only one type of lamellar crystal with a d_{ac} of 14.5 nm and d_c of 8.3 nm (Figure S6f), reflecting that the lamellar thickness of iPP-1 is less sensitive to the thermomechanical field during injection molding. The evolution of the shish structure of HDPE-1 and iPP-1 is also

https://doi.org/10.1021/acs.macromol.3c00194
Macromolecules XXXX, XXX, XXX−XXX

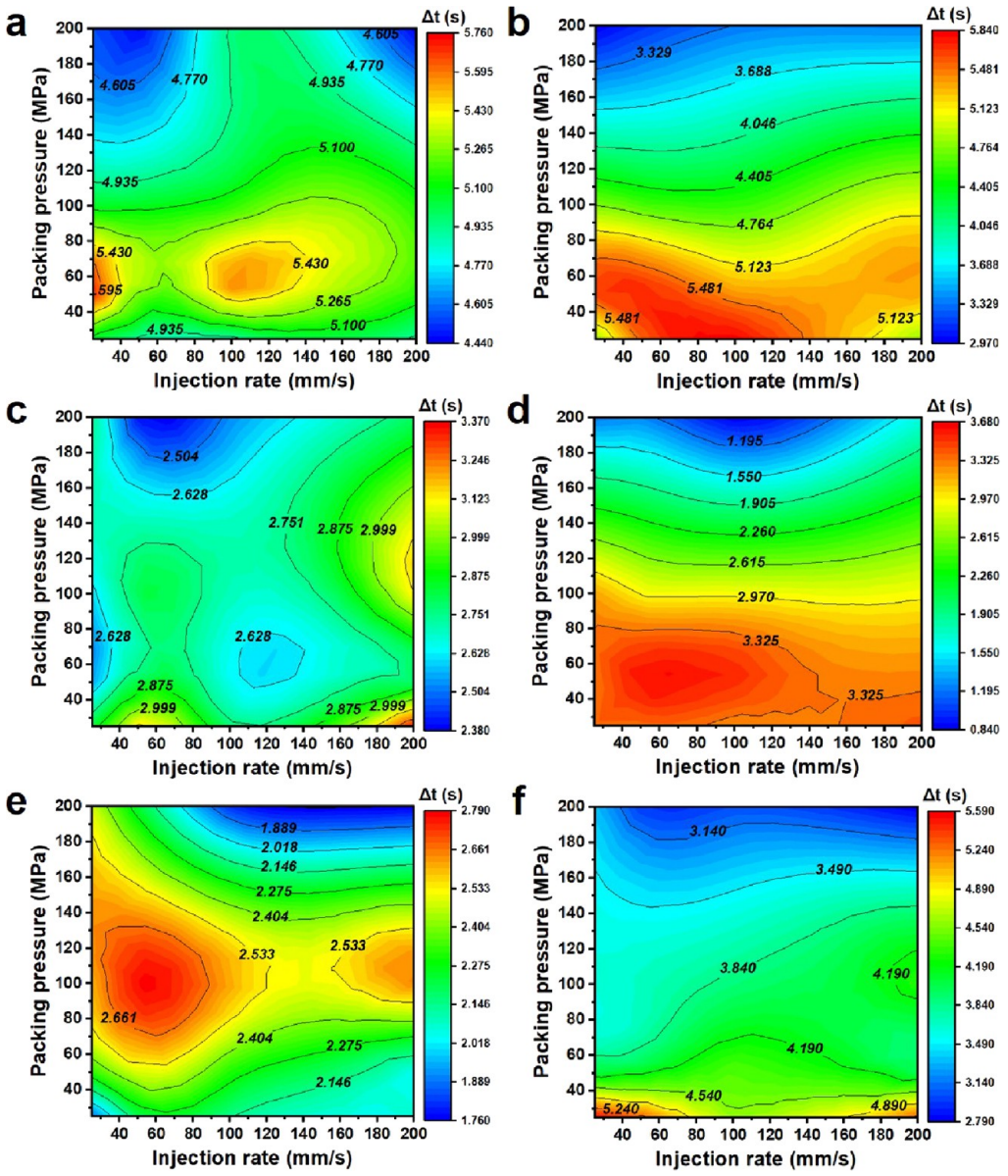

Figure 5. Contour maps of the crystallization time (Δt) as the function of injection molding parameters. α crystals of (a) HDPE-1, (b) HDPE-2, (c) iPP-1, (d) iPP-2, and (e) iPP-1/β. (f) β crystals of iPP-1/β.

shown in Figures S8 and S9, respectively. It is found that the shear-induced precursor is formed and subsequently transformed into the shish structure quickly within 0.1 s. It can also be found from 2D-SAXS patterns of both HDPE-1 and iPP-1 that the scattering intensities of the shish increase first and then decrease with time. We believe that, at the beginning of injection molding, oriented shish structures are formed in HDPE-1 and iPP-1 melts induced by the intensive shear flow, and when an instantaneous shear effect disappears, the oriented chain or shish structure will relax during the subsequent cooling process, which leads to the weakening of the shish scattering intensities. Comparing the shish formation of HDPE-1 and iPP-1, it is known that the shish structure of HDPE-1 occurs earlier than that of iPP-1 with time during injection molding, indicating that chain segments of the HDPE-1 has higher sensitivity than that of iPP-1 to the thermomechanical field during injection molding due to the fact that the HDPE-1 macromolecular chain is more flexible and shear-sensitive. The average length (L_{shish}) of shish structure of HDPE-1 and iPP-1 is calculated quantitatively (Figure S10). The L_{shish} of HDPE-1 is 73.53 nm, which is larger than that of iPP-1 with 37.75 nm, indicating that HDPE-1 molecularly chains to align and orient themselves along the flow field direction to form shish structures due to high chain flexibility, which is consistent with the above analysis. Additionally, both the long periods of HDPE-1 and iPP-1 present an increase first at the packing stage due to crystallization and the decline of the packing pressure; subsequently, a decrease of the long period at the cooling stage is attributed to material shrinkage (Figure 4b,d).

During injection molding, there is not only the growth of lamellar crystals but also the orientation of lamellar crystals. The variation of the orientation degree of two types of lamellae for HDPE-1 during injection molding is shown in Figure S11. Notably, the orientation degree of thick lamellar crystals is higher than that of the thin lamellar crystals before the cooling stage and, subsequently, the orientation degrees of two kinds of lamellar crystals tend to be close. This observation also verifies

https://doi.org/10.1021/acs.macromol.3c00194
Macromolecules XXXX, XXX, XXX−XXX

our speculation that the strong shear flow and high pressure promote the orientation of chain segments along the flow direction to crystallize into shish, which serve as the nucleation sites for the growth of kebabs (i.e., thick lamellar crystals) at the early stage of crystallization, but in the later stage, epitaxially lamellar crystals (i.e., thin lamellar crystals) grow on the surface of the shish-kebab structure, resulting in the reduction of the overall orientation degree. In summary, the strong shear flow during the filling stage induces a high orientation degree of molecular chains and, subsequently, the shish-kebab structure could form at high temperatures, which is favorable for the formation of thick lamellae. Moreover, the packing pressure could also promote lamella thickening. It is highly possible that the formation of thin lamellae contributes to the epitaxial growth of lamellae on the shish-kebab structure. As for the case of iPP-1, the orientation degree of lamellar crystals presents the same tendency with that of HDPE-1. However, it is generally thinner than that of HDPE-1 (Figure S12). Except for HDPE-1 and iPP-1, the in situ characterization system of injection molding can also identify the formation and evolution of the lamellar structures of various polyolefins under different processing conditions (Figure S13), showing a universal feature for the study on the growth and orientation of folded-chain lamellar crystals of semicrystalline polymers.

3.5. High-Throughput Determination of Process Windows for Polymer Injection Molding. Aiming to quickly determine feasible process conditions for the achievement of the qualified molded parts, the determination of the processing window for the injection molding of certain polymer materials is valuable for the achievement of the qualified molded parts and high molding efficiency in industry.[64] However, it is usually of high labor costs and requires a mass of experimental data to establish the process window. Therefore, huge amounts of empirical trials are required to be carried out iteratively with a low efficiency. Except for experimental trials, some researchers attempt to determine the window by a number of finite element simulation methods with different combinations of molding parameters. However, the mathematical model of each stage for the injection molding is usually simplified for convenient calculation, leading to the simulated results deviating from a real situation of injection molding. Therefore, the accuracy of the obtained process window still needs to be verified by experimental trails.[65,66] On the other hand, the complicated model with desirable accuracy needs the establishment of the more finite element meshes, which leads to a lot of computational time and a matched computer with ultrafast running speed. The in situ characterization system of injection molding could directly identify the crystallization time for various processing parameters, which could be a promising tool to achieve a mapping of the processing windows in a high-throughput manner. The characteristic parameter of the processing efficiency, namely, the crystallization time (Δt), defined as the interval from the on-set of (110) plane growth to the maximum intensity of diffraction as shown in previous sections, is plotted against the packing pressure and injection rate in a two-coordinate diagram, and the results are shown in Figure 5. The quantified crystallization time can be obtained directly and the optimal processing conditions of certain polymers during injection molding can be identified conveniently by a crystallization time map as a function of injection molding parameters.

As shown in Figure 5, the "red region" represents the processing conditions that slow down the crystallization process of polymers and the "blue region" means that the processing conditions accelerate the crystallization of polymers. Generally, the high packing pressure shortens the crystallization time and facilitates the crystal growth of HDPE and iPP. In contrast, the injection rate does not have a significant effect on the crystallization time. Multi-processing fields in injection molding are coupled with the types of materials, leading to a typically non-linear relationship between the processing and structure. To sum up, although the underlying physics is still needed to be investigated further, such an in situ characterization system is helpful for mapping processing windows of injection molding in a high through-put way.

4. CONCLUSIONS

In this work, a high-throughput and in situ characterization system for industrial injection molding is built for the first time. This system can investigate the rapid evolution of multiscale and multilevel structures of polymers under the complex thermomechanical field during injection molding simultaneously. The novel crystallization behaviors of HDPE and iPP such as the crystallization kinetics, polymorphism evolution, and growth and orientation of lamellar crystals are revealed systematically and efficiently via this system. Meanwhile, the in situ characterization is successfully utilized to efficiently quantify the crystallization time under various processing conditions of injection molding, and processing windows are established directly. Compared to the traditional "black box" research paradigm of injection molding, this work provides a research platform for efficient acquisition of the hierarchically crystalline structure during injection molding of semicrystalline polymers and directly determines a quantitative processing window for specific polymer injection molding. It is highly expected to provide direct guidance for injection molding manufacturing in industry. Note that some improvements of this characterization system are possible. The mold temperature is crucial to injection molding in industry in order to investigate different types of polymers such as engineering plastics, and the mold temperature especially at a high temperature will be realized by using a clean heating medium in the future. In addition, the in situ characterization system of injection molding has revealed the average results of WAXD or SAXS during injection molding. Since the skin−core structure appears sometimes, therefore, X-ray scattering technology with a high spatial resolution will be attempted to study the skin−core structure of polymer during injection molding.

■ ASSOCIATED CONTENT

Supporting Information

The Supporting Information is available free of charge at https://pubs.acs.org/doi/10.1021/acs.macromol.3c00194.

Simulation of the temperature, shear, and pressure fields during injection molding of HDPE-1 and iPP-1; crystal growth of HDPE-1 and iPP-1 during injection molding; lattice spacing of HDPE-1 and iPP-1 crystals; comparison of K_β values and (110) plane crystallization rates (G) of iPP-1 and iPP-1/β at different melt-processing temperatures; growth processes of α (110) and β (110) in iPP-1/β at different packing pressures; 2D-SAXS patterns and the corresponding 1D-SAXS curves of

https://doi.org/10.1021/acs.macromol.3c00194
Macromolecules XXXX, XXX, XXX−XXX

HDPE-1 and iPP-1; comparison of thermal behavior for HDPE-1 and iPP-1; selected 2D-SAXS patterns of HDPE-1 as a function of time during injection molding; selected 2D-SAXS patterns of iPP-1 as a function of time during injection molding; plots of the azimuthal width (B_{obs}) as a function of 1/s, which is used to determine the average length of shish (L_{shish}); orientation degree of two lamellar crystals for HDPE-1; orientation degree of the lamellar crystal for iPP-1; and contour maps of 1D-SAXS azimuthal intensity distribution curves reflecting the orientation degree of the lamellar crystal of different polymers (PDF)

The structural evolution of the α crystal of HDPE-1 during injection molding is detected by the WAXS detector with exposure time of 0.025 s with injection rate of 100 mm/s and pressure of 200 MPa (MP4)

The structural evolution of the α crystal and β crystal of iPP-1 during injection molding is detected by the WAXS detector with an exposure time of 0.025 s with an injection rate of 100 mm/s and pressure of 200 MPa (MP4)

The structural evolution of the α crystal and β crystal of iPP-1 with β-NA during injection molding is detected by the WAXS detector with an exposure time of 0.025 s with an injection rate of 100 mm/s and pressure of 100 MPa (MP4)

The growth process of the two folded-chain lamellar crystals of HDPE-1 during injection molding is detected by the SAXS detector with an exposure time of 0.025 s with an injection rate of 100 mm/s and pressure of 200 MPa (MP4)

The growth process of the folded-chain lamellar crystal of iPP-1 during injection molding is detected by the SAXS detector with an exposure time of 0.025 s with an injection rate of 100 mm/s and pressure of 200 MPa (MP4)

AUTHOR INFORMATION

Corresponding Authors

Gan-Ji Zhong − *College of Polymer Science and Engineering, State Key Laboratory of Polymer Materials Engineering, Sichuan University, Chengdu 610065, China;* orcid.org/0000-0002-8540-7293; Phone: +86-28-8540-0211; Email: ganji.zhong@scu.edu.cn; Fax: +86-28-8540-6866

Zhong-Ming Li − *College of Polymer Science and Engineering, State Key Laboratory of Polymer Materials Engineering, Sichuan University, Chengdu 610065, China;* orcid.org/0000-0001-7203-1453; Email: zmli@scu.edu.cn

Authors

Jin Yin − *College of Polymer Science and Engineering, State Key Laboratory of Polymer Materials Engineering, Sichuan University, Chengdu 610065, China*

Lu-Feng Deng − *College of Polymer Science and Engineering, State Key Laboratory of Polymer Materials Engineering, Sichuan University, Chengdu 610065, China*

Guo-Qi Ma − *College of Polymer Science and Engineering, State Key Laboratory of Polymer Materials Engineering, Sichuan University, Chengdu 610065, China*

Feng-Yang Wu − *College of Polymer Science and Engineering, State Key Laboratory of Polymer Materials Engineering, Sichuan University, Chengdu 610065, China*

Jia-Zhuang Xu − *College of Polymer Science and Engineering, State Key Laboratory of Polymer Materials Engineering, Sichuan University, Chengdu 610065, China;* orcid.org/0000-0001-9888-7014

Xueqin Gao − *College of Polymer Science and Engineering, State Key Laboratory of Polymer Materials Engineering, Sichuan University, Chengdu 610065, China;* orcid.org/0000-0003-2481-5581

Fenggang Bian − *Shanghai Synchrotron Radiation Facility, Shanghai Advanced Research Institute, Chinese Academy of Sciences, Shanghai 201204, China*

Jun Lei − *College of Polymer Science and Engineering, State Key Laboratory of Polymer Materials Engineering, Sichuan University, Chengdu 610065, China;* orcid.org/0000-0001-6803-5216

Complete contact information is available at: https://pubs.acs.org/10.1021/acs.macromol.3c00194

Author Contributions

[#]J.Y. and L.-F. D. contributed equally to this work.

Notes

The authors declare no competing financial interest.

ACKNOWLEDGMENTS

This work is supported by the National Key R&D Program of China (no. 2018YFB0704200), the National Natural Science Foundation of China (grant nos. 52033005, 52173040, and 52173225), the Foundation of Science & Technology Department of Sichuan Province (grant no. 21CXRC0105), and the fund from Sichuan University (no. 2022SCUH0039). We also thank Beamline BL10U1 in SSRF for supporting the X-ray measurement and Qian Liu for helping with the experiment.

REFERENCES

(1) Maghsoudi, K.; Jafari, R.; Momen, G.; Farzaneh, M. Micro-nanostructured polymer surfaces using injection molding: A review. *Mater. Today Commun.* **2017**, *13*, 126−143.

(2) Pantani, R.; Speranza, V.; Titomanlio, G. Thirty Years of Modeling of Injection Molding. A Brief Review of the Contribution of UNISA Code to the Field. *Int. Polym. Process.* **2016**, *31*, 655−663.

(3) Watanabe, K.; Suzuki, T.; Masubuchi, Y.; Taniguchi, T.; Takimoto, J.-i.; Koyama, K. Crystallization kinetics of polypropylene under high pressure and steady shear flow. *Polymer* **2003**, *44*, 5843−5849.

(4) Zhao, X.; Liao, T.; Yang, X.; Coates, P.; Whiteside, B.; Barker, D.; Thompson, G.; Jiang, Z.; Men, Y. Mold temperature- and molar mass-dependent structural formation in micro-injection molding of isotactic polypropylene. *Polymer* **2022**, *248*, 124797−124806.

(5) Liao, T.; Zhao, X.; Yang, X.; Coates, P.; Whiteside, B.; Barker, D.; Thompson, G.; Lai, Y.; Jiang, Z.; Men, Y. In situ synchrotron small angle X-ray scattering investigation of structural formation of polyethylene upon micro-injection molding. *Polymer* **2021**, *215*, 123390−123397.

(6) Dumitrescu, O. R.; Baker, D. C.; Foster, G. M.; Evans, K. E. Near infrared spectroscopy for in-line monitoring during injection moulding. *Polym. Test.* **2005**, *24*, 367−375.

(7) Favaro, M. M.; Marinelli, A. L.; Farah, M.; Bretas, R. E. S. Optical monitoring of polypropylene crystallization during injection molding. *Polym. Eng. Sci.* **2008**, *48*, 257−266.

(8) Moretti, F.; Favaro, M. M.; Branciforti, M. C.; Bretas, R. E. S. Optical monitoring of the injection molding of intercalated polypropylene nanocomposites. *Polym. Eng. Sci.* **2010**, *50*, 1326−1339.

(9) Shelton, C. K.; Jones, R. L.; Epps, T. H. Kinetics of Domain Alignment in Block Polymer Thin Films during Solvent Vapor Annealing with Soft Shear: An in Situ Small-Angle Neutron Scattering Investigation. *Macromolecules* **2017**, *50*, 5367−5376.
(10) Cui, K.; Ma, Z.; Tian, N.; Su, F.; Liu, D.; Li, L. Multiscale and Multistep Ordering of Flow-Induced Nucleation of Polymers. *Chem. Rev.* **2018**, *118*, 1840−1886.
(11) Yang, S. G.; Wei, Z. Z.; Cseh, L.; Kazemi, P.; Zeng, X. B.; Xie, H. J.; Saba, H.; Ungar, G. Bowls, vases and goblets-the microcrockery of polymer and nanocomposite morphology revealed by two-photon optical tomography. *Nat. Commun.* **2021**, *12*, 5054−5061.
(12) Feng, L. Z.; Wang, J. J.; Ma, T.; Yin, Y. C.; Song, K. H.; Li, Z. D.; Zhou, M. M.; Jin, S.; Zhuang, T.; Fan, F. J.; et al. Biomimetic non-classical crystallization drives hierarchical structuring of efficient circularly polarized phosphors. *Nat. Commun.* **2022**, *13*, 3339−3348.
(13) Pantani, R.; Coccorullo, I.; Speranza, V.; Titomanlio, G. Modeling of morphology evolution in the injection molding process of thermoplastic polymers. *Prog. Polym. Sci.* **2005**, *30*, 1185−1222.
(14) Yang, C.-F.; Huang, Y.-F.; Ruan, J.; Su, A.-C. Extensive Development of Precursory Helical Pairs Prior to Formation of Stereocomplex Crystals in Racemic Polylactide Melt Mixture. *Macromolecules* **2012**, *45*, 872−878.
(15) Zhang, X.-X.; Yang, S.-G.; Zhong, G.-J.; Lei, J.; Liu, D.; Sun, G.-A.; Xu, J.-Z.; Li, Z.-M. Rapid Melt Crystallization of Bisphenol-A Polycarbonate Jointly Induced by Pressure and Flow. *Macromolecules* **2021**, *54*, 2383−2393.
(16) Kimata, S.; Sakurai, T.; Nozue, Y.; Kasahara, T.; Yamaguchi, N.; Karino, T.; Shibayama, M.; Kornfield, J. A. Molecular basis of the shish-kebab morphology in polymer crystallization. *Science* **2007**, *316*, 1014−1017.
(17) Huang, Y.; Rui, G.; Li, Q.; Allahyarov, E.; Li, R.; Fukuto, M.; Zhong, G. J.; Xu, J. Z.; Li, Z. M.; Taylor, P. L.; Zhu, L. Enhanced piezoelectricity from highly polarizable oriented amorphous fractions in biaxially oriented poly(vinylidene fluoride) with pure beta crystals. *Nat. Commun.* **2021**, *12*, 675−682.
(18) Lin, Y.; Chen, W.; Meng, L.; Wang, D.; Li, L. Recent advances in post-stretching processing of polymer films with in situ synchrotron radiation X-ray scattering. *Soft Matter* **2020**, *16*, 3599−3612.
(19) Hu, T.; Hua, W.-Q.; Zhong, G.-J.; Wang, Y.-D.; Gao, Y.-T.; Hong, C.-X.; Li, Z.-M.; Bian, F.-G.; Xiao, T.-Q. Nondestructive and Quantitative Characterization of Bulk Injection-Molded Polylactide Using SAXS Microtomography. *Macromolecules* **2020**, *53*, 6498−6509.
(20) Rodríguez-Ruiz, I.; Radajewski, D.; Charton, S.; Phamvan, N.; Brennich, M.; Pernot, P.; Bonneté, F.; Teychené, S. Innovative High-Throughput SAXS Methodologies Based on Photonic Lab-on-a-Chip Sensors: Application to Macromolecular Studies. *Sensors* **2017**, *17*, 1266−1277.
(21) Liu, D.; Tian, N.; Huang, N.; Cui, K.; Wang, Z.; Hu, T.; Yang, H.; Li, X.; Li, L. Extension-Induced Nucleation under Near-Equilibrium Conditions: The Mechanism on the Transition from Point Nucleus to Shish. *Macromolecules* **2014**, *47*, 6813−6823.
(22) Chang, J.; Wang, Z.; Tang, X.; Tian, F.; Ye, K.; Li, L. A portable extruder for in situ wide angle x-ray scattering study on multi-dimensional flow field induced crystallization of polymer. *Rev. Sci. Instrum.* **2018**, *89*, 025101−025107.
(23) Rendon, S.; Fang, J.; Burghardt, W. R.; Bubeck, R. A. An apparatus for in situ x-ray scattering measurements during polymer injection molding. *Rev. Sci. Instrum.* **2009**, *80*, 043902−043910.
(24) Oztemel, E.; Gursev, S. Literature review of Industry 4.0 and related technologies. *J. Intell. Manuf.* **2020**, *31*, 127−182.
(25) Zhong, R. Y.; Xu, X.; Klotz, E.; Newman, S. T. Intelligent Manufacturing in the Context of Industry 4.0: A Review. *Engineering* **2017**, *3*, 616−630.
(26) Hong, S.; Liow, C. H.; Yuk, J. M.; Byon, H. R.; Yang, Y.; Cho, E.; Yeom, J.; Park, G.; Kang, H.; Kim, S.; Shim, Y.; Na, M.; Jeong, C.; Hwang, G.; Kim, H.; Kim, H.; Eom, S.; Cho, S.; Jun, H.; Lee, Y.; Baucour, A.; Bang, K.; Kim, M.; Yun, S.; Ryu, J.; Han, Y.; Jetybayeva, A.; Choi, P. P.; Agar, J. C.; Kalinin, S. V.; Voorhees, P. W.; Littlewood, P.; Lee, H. M. Reducing Time to Discovery: Materials and Molecular Modeling, Imaging, Informatics, and Integration. *ACS Nano* **2021**, *15*, 3971−3995.
(27) Batra, R.; Song, L.; Ramprasad, R. Emerging materials intelligence ecosystems propelled by machine learning. *Nat. Rev. Mater.* **2021**, *6*, 655−678.
(28) Jablonka, K. M.; Ongari, D.; Moosavi, S. M.; Smit, B. Big-Data Science in Porous Materials: Materials Genomics and Machine Learning. *Chem. Rev.* **2020**, *120*, 8066−8129.
(29) Zhao, Y.; Zhang, J.; Xu, Z.; Sun, S.; Langner, S.; Hartono, N. T. P.; Heumueller, T.; Hou, Y.; Elia, J.; Li, N.; Matt, G. J.; Du, X.; Meng, W.; Osvet, A.; Zhang, K.; Stubhan, T.; Feng, Y.; Hauch, J.; Sargent, E. H.; Buonassisi, T.; Brabec, C. J. Discovery of temperature-induced stability reversal in perovskites using high-throughput robotic learning. *Nat. Commun.* **2021**, *12*, 2191−2199.
(30) Hitt, J. L.; Li, Y. C.; Tao, S.; Yan, Z.; Gao, Y.; Billinge, S. J. L.; Mallouk, T. E. A high throughput optical method for studying compositional effects in electrocatalysts for CO_2 reduction. *Nat. Commun.* **2021**, *12*, 1114−1120.
(31) Lu, R.; Neff, N. F.; Quake, S. R.; Weissman, I. L. Tracking single hematopoietic stem cells in vivo using high-throughput sequencing in conjunction with viral genetic barcoding. *Nat. Biotechnol.* **2011**, *29*, 928−933.
(32) He, B.; Zhang, X.; Zhang, Q.; Fu, Q. Real-time ultrasonic monitoring of the injection-molding process. *J. Appl. Polym. Sci.* **2008**, *107*, 94−101.
(33) Nie, C.; Peng, F.; Xu, T.; Ding, Y.; Sheng, J.; Chen, W.; Li, L. Biaxial Stretch-Induced Crystallization of Polymers: A Molecular Dynamics Simulation Study. *Macromolecules* **2021**, *54*, 9794−9803.
(34) Carmeli, E.; Kandioller, G.; Gahleitner, M.; Müller, A. J.; Tranchida, D.; Cavallo, D. Continuous Cooling Curve Diagrams of Isotactic-Polypropylene/Polyethylene Blends: Mutual Nucleating Effects under Fast Cooling Conditions. *Macromolecules* **2021**, *54*, 4834−4846.
(35) Luo, S.; Li, N.; Zhang, S.; Zhang, C.; Qu, T.; Ocheje, M. U.; Xue, G.; Gu, X.; Rondeau-Gagné, S.; Hu, W.; Wang, S.; Teng, C.; Zhou, D.; Xu, J. Observation of Stepwise Ultrafast Crystallization Kinetics of Donor−Acceptor Conjugated Polymers and Correlation with Field Effect Mobility. *Chem. Mater.* **2021**, *33*, 1637−1647.
(36) Schulz, M.; Schäfer, M.; Saalwächter, K.; Thurn-Albrecht, T. Competition between crystal growth and intracrystalline chain diffusion determines the lamellar thickness in semicrystalline polymers. *Nat. Commun.* **2022**, *13*, 119−128.
(37) Ma, Z.; Balzano, L.; Peters, G. W. M. Pressure Quench of Flow-Induced Crystallization Precursors. *Macromolecules* **2012**, *45*, 4216−4224.
(38) Kearns, K. L.; Scherzer, J.; Chyasnavichyus, M.; Monaenkova, D.; Moore, J.; Sammler, R. L.; Fielitz, T.; Nicholson, D. A.; Andreev, M.; Rutledge, G. C. Measuring Flow-Induced Crystallization Kinetics of Polyethylene after Processing. *Macromolecules* **2021**, *54*, 2101−2112.
(39) Somani, R. H.; Hsiao, B. S.; Nogales, A.; Fruitwala, H.; Srinivas, S.; Tsou, A. H. Structure Development during Shear Flow Induced Crystallization of i-PP: In Situ Wide-Angle X-ray Diffraction Study. *Macromolecules* **2001**, *34*, 5902−5909.
(40) Yang, S.-G.; Chen, Y.-H.; Deng, B.-W.; Lei, J.; Li, L.; Li, Z.-M. Window of Pressure and Flow To Produce β-Crystals in Isotactic Polypropylene Mixed with β-Nucleating Agent. *Macromolecules* **2017**, *50*, 4807−4816.
(41) Jauncey, G. E. The Scattering of X-Rays and Braggs Law. *Proc. Natl. Acad. Sci. U. S. A.* **1924**, *10*, 57−60.
(42) Tashiro, K.; Sasaki, S.; Kobayashi, M. Structural Investigation of Orthorhombic-to-Hexagonal Phase Transition in Polyethylene Crystal: The Experimental Confirmation of the Conformationally Disordered Structure by X-ray Diffraction and Infrared/Raman Spectroscopic Measurements. *Macromolecules* **1996**, *29*, 7460−7469.
(43) Tsubakihara, S.; Nakamura, A.; Yasuniwa, M. Hexagonal Phase of Polyethylene Fibers under High-Pressure. *Polym. J.* **1991**, *23*, 1317−1324.

https://doi.org/10.1021/acs.macromol.3c00194
Macromolecules XXXX, XXX, XXX−XXX

(44) Hikosaka, M.; Rastogi, S.; Keller, A.; Kawabata, H. Investigations on the crystallization of polyethylene under high pressure: Role of mobile phases, lamellar thickening growth, phase transformations, and morphology. *J. Macromol. Sci., Part B: Phys.* **1992**, *31*, 87−131.
(45) Chen, Y.-H.; Zhong, G.-J.; Wang, Y.; Li, Z.-M.; Li, L. Unusual Tuning of Mechanical Properties of Isotactic Polypropylene Using Counteraction of Shear Flow and β-Nucleating Agent on β-Form Nucleation. *Macromolecules* **2009**, *42*, 4343−4348.
(46) Chen, Y.-H.; Mao, Y.-M.; Li, Z.-M.; Hsiao, B. S. Competitive Growth of α- and β-Crystals in β-Nucleated Isotactic Polypropylene under Shear Flow. *Macromolecules* **2010**, *43*, 6760−6771.
(47) Zhang, B.; Wang, B.; Chen, J.; Shen, C.; Reiter, R.; Chen, J.; Reiter, G. Flow-Induced Dendritic β-Form Isotactic Polypropylene Crystals in Thin Films. *Macromolecules* **2016**, *49*, 5145−5151.
(48) Zhao, S.; Cai, Z.; Xin, Z. A highly active novel β-nucleating agent for isotactic polypropylene. *Polymer* **2008**, *49*, 2745−2754.
(49) Varga, J. β-Modification of Isotactic Polypropylene: Preparation, Structure, Processing, Properties, and Application. *J. Macromol. Sci., Part B: Phys.* **2002**, *41*, 1121−1171.
(50) Meille, S. V.; Ferro, D. R.; Brueckner, S.; Lovinger, A. J.; Padden, F. J. Structure of β-Isotactic Polypropylene: A Long-Standing Structural Puzzle. *Macromolecules* **1994**, *27*, 2615−2622.
(51) Luo, F.; Geng, C.; Wang, K.; Deng, H.; Chen, F.; Fu, Q.; Na, B. New Understanding in Tuning Toughness of β-Polypropylene: The Role of β-Nucleated Crystalline Morphology. *Macromolecules* **2009**, *42*, 9325−9331.
(52) Cai, Z.; Zhang, Y.; Li, J.; Xue, F.; Shang, Y.; He, X.; Feng, J.; Wu, Z.; Jiang, S. Real time synchrotron SAXS and WAXS investigations on temperature related deformation and transitions of β-iPP with uniaxial stretching. *Polymer* **2012**, *53*, 1593−1601.
(53) Varga, J.; Karger-Kocsis, J. Rules of supermolecular structure formation in sheared isotactic polypropylene melts. *J. Polym. Sci., Part B: Polym. Phys.* **1996**, *34*, 657−670.
(54) Liu, L.; Zhao, Y.; Zhang, C.; Dong, Z.; Wang, K.; Wang, D. Morphological Characteristics of β-Nucleating Agents Governing the Formation of the Crystalline Structure of Isotactic Polypropylene. *Macromolecules* **2021**, *54*, 6824−6834.
(55) Cai, Z.; Zhang, Y.; Li, J.; Shang, Y.; Huo, H.; Feng, J.; Funari, S. S.; Jiang, S. Temperature-dependent selective crystallization behavior of isotactic polypropylene with a β-nucleating agent. *J. Appl. Polym. Sci.* **2013**, *128*, 628−635.
(56) Stocker, W.; Schumacher, M.; Graff, S.; Thierry, A.; Wittmann, J.-C.; Lotz, B. Epitaxial Crystallization and AFM Investigation of a Frustrated Polymer Structure: Isotactic Poly(propylene), β Phase. *Macromolecules* **1998**, *31*, 807−814.
(57) Varga, J.; Menyhárd, A. Effect of Solubility and Nucleating Duality of N,N-Dicyclohexyl-2,6-naphthalenedicarboxamide on the Supermolecular Structure of Isotactic Polypropylene. *Macromolecules* **2007**, *40*, 2422−2431.
(58) Dong, M.; Jia, M.-y.; Guo, Z.-x.; Yu, J. Effect of final heating temperature on crystallization of isotactic polypropylene nucleated with an aryl amide derivative as β-form nucleating agent. *Chin. J. Polym. Sci.* **2011**, *29*, 308−317.
(59) Luo, F.; Wang, K.; Ning, N.; Geng, C.; Deng, H.; Chen, F.; Fu, Q.; Qian, Y.; Zheng, D. Dependence of mechanical properties on β-form content and crystalline morphology for β-nucleated isotactic polypropylene. *Polym. Adv. Technol.* **2011**, *22*, 2044−2054.
(60) Li, Y.; Wen, X.; Nie, M.; Wang, Q. Controllable reinforcement of stiffness and toughness of polypropylene via thermally induced self-assembly of β-nucleating agent. *J. Appl. Polym. Sci.* **2014**, *131*, 40605−40613.
(61) van Drongelen, M.; van Erp, T. B.; Peters, G. W. M. Quantification of non-isothermal, multi-phase crystallization of isotactic polypropylene: The influence of cooling rate and pressure. *Polymer* **2012**, *53*, 4758−4769.
(62) Yang, H.-R.; Lei, J.; Li, L.; Fu, Q.; Li, Z.-M. Formation of Interlinked Shish-Kebabs in Injection-Molded Polyethylene under the Coexistence of Lightly Cross-Linked Chain Network and Oscillation Shear Flow. *Macromolecules* **2012**, *45*, 6600−6610.
(63) Yang, L.; Somani, R. H.; Sics, I.; Hsiao, B. S.; Kolb, R.; Fruitwala, H.; Ong, C. Shear-Induced Crystallization Precursor Studies in Model Polyethylene Blends by in-Situ Rheo-SAXS and Rheo-WAXD. *Macromolecules* **2004**, *37*, 4845−4859.
(64) Fernandes, C.; Pontes, A. J.; Viana, J. C.; Gaspar-Cunha, A. Modeling and Optimization of the Injection-Molding Process: A Review. *Adv. Polym. Technol.* **2018**, *37*, 429−449.
(65) Zhao, P.; Zhang, J.; Dong, Z.; Huang, J.; Zhou, H.; Fu, J.; Turng, L.-S. Intelligent Injection Molding on Sensing, Optimization, and Control. *Adv. Polym. Technol.* **2020**, *2020*, 1−22.
(66) Yamamoto, T. Molecular Dynamics of Crystallization in a Helical Polymer Isotactic Polypropylene from the Oriented Amorphous State. *Macromolecules* **2014**, *47*, 3192−3202.

https://doi.org/10.1021/acs.macromol.3c00194
Macromolecules XXXX, XXX, XXX−XXX